Available online at www.sciencedirect.com
SCIENCE DIRECT®
Catalysis Today 90 (2004) 277–281
CATALYSIS TODAY
www.elsevier.com/locate/cattod

Efficient usage of highly dispersed Pt on carbon nanotubes for electrode catalysts of polymer electrolyte fuel cells

T. Matsumoto [a], T. Komatsu [a], H. Nakano [a,1], K. Arai [a], Y. Nagashima [a], E. Yoo [a], T. Yamazaki [a], M. Kijima [a], H. Shimizu [b], Y. Takasawa [b], J. Nakamura [a,*]

[a] *Institute of Materials Science, University of Tsukuba, Tsukuba, Japan*
[b] *NBO Development Center, Sekisui Chemical Co., LTD., 32 Wadai, Tsukuba, Ibaraki 300-4292, Japan*

Abstract

A Pt-deposited carbon nanotube (CNT) shows higher performance than a commercial Pt-deposited carbon black (CB) with reducing 60% Pt load per electrode area in polymer electrolyte fuel cells (PEFCs) below 500 mA/cm^2. K_2PtCl_4 and $H_2PtCl_6{\cdot}6(H_2O)$ are used for the Pt deposition onto multi-walled CNTs (MWCNTs), which are produced by the catalytic decomposition of hydrocarbons. The electric power densities produced using the Pt/CNT electrodes are greater than that of the Pt/CB by a factor of two to four on the basis of the Pt load per power. CNTs are thus found to be a good support of Pt particles for PEFC electrodes. TEM images show 2–4-nm Pt nanoparticles dispersed on the CNT surfaces. These high performances are considered to be due to the efficient formation of the triple-phase boundaries of gas–electrode–electrolyte. The mechanisms of Pt deposition are discussed for these Pt-deposited CNTs.

Keywords: Carbon; Nanotube; Pt; Fuel cell; Electrode; TEM; IR

1. Introduction

High electric power is produced by polymer electrolyte fuel cells (PEFCs) with low weight, cost, volume, and environmental load [1]. The low temperature is another advantage of PEFC because of the fast start-up. The best catalysts in the present PEFC technology are Pt and Pt–Ru, but are expensive and insufficient to commercialize as a resources [1]. The efficient Pt loading is thus an important technique for the development of PEFC. One of the possibilities is the application of carbon nanotubes (CNTs) as a support of Pt catalysts. Large surface areas are available on Pt nanoparticles per Pt atom compared to thin Pt films, and the CNTs are convenient supports for keeping Pt particles dispersed [1–6]. The carbon black (CB) has been used as the Pt supports, where the problem of Pt/CB is that the Pt particles are trapped in deep cracks of CB, which are the crystal boundaries of the small carbon particles consisting of CB [7]. Such particles cannot work as catalysts of electrodes because the effective formation of the triple-phase boundary (gas–electrode–electrolyte) is essential for PEFC. The CNTs do not have such cracks so that most Pt particles are expected to be used as effective catalysts. Another prospect is that the network constructed by CNTs is considered to be micropores or gas lines resulting in the high performance of anode [1]. The superiority to CB has been reported for not only the CNTs [2,3] but also carbon nanohorns (CNHs) [8].

In this study, the Pt/CNTs are prepared with $H_2PtCl_6{\cdot}6(H_2O)$ and K_2PtCl_4, and the performance as electrode catalysts is measured by comparing to a commercial Pt/CB catalyst. The Pt/CNT catalysts are then characterized by TEM, IR, and XPS to discuss the Pt deposition mechanisms.

2. Experimental

The CNTs (Shenzhen Nanotech Co. Ltd.) produced by catalytic decomposition of hydrocarbons were purified by the ultrasonic treatment for 1 h, refluxed in 14 N HNO_3 at 423 K for 2 h, poured into distilled water, and filtered with a 200-nm membrane as the pretreatment.

The electrode catalysts of Pt-deposited CNTs were prepared with two Pt compounds of $H_2Pt^{IV}Cl_6{\cdot}6(H_2O)$ or $K_2Pt^{II}Cl_4$ (30 wt.%). CNTs were heated and stirred with

* Correspondig author. Tel.: +81-29-853-5279; fax: +81-29-853-5279.
E-mail address: nakamura@ims.tsukuba.ac.jp (J. Nakamura).
[1] Present address: ULVAC-PHI, Japan.

0920-5861/$ – see front matter © 2004 Elsevier B.V. All rights reserved.
doi:10.1016/j.cattod.2004.04.038

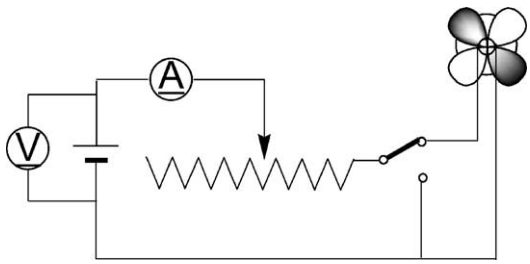

Fig. 1. Circuit for the *I–V* curve measurement. The resistance is variable and the current can be checked by eyes.

$H_2PtCl_6{\cdot}6(H_2O)$ (30 wt.%) in ethylene glycol at 313 K for 2 h. This solution was added into HNO_3 (14 N, 50 ml), dissoluted into 400 ml of distilled water, and filtered. The filtered water was almost as yellow as the H_2PtCl_6 solution. This sample is denoted as HPt-CNT here. This procedure has often been applied for the Pt deposition on carbon supports [2–5]. The following treatment was applied for K_2PtCl_4, which is labeled as KPt-CNT. The 1-g CNTs were stirred in the mixture of HNO_3 (14 N, 50 ml) and H_2SO_4 (98%, 50 ml) for 12 h to make defect sites in CNTs [9,10]. This solution was added into HNO_3 (14 N, 50 ml), sonicated, dissoluted into 400 ml of distilled water, and filtered. The oxidized CNTs were stirred in distilled water with adding K_2PtCl_4 (30 wt.%) in ethanol, and refluxed at 373 K for 2 h in a dark room. The filtered water was colorless though the K_2PtCl_4 solution was originally brown before adding CNTs. A commercial 29 wt.% Pt-deposited CB (Tanaka Kikinzoku Kogyo) [11,12] was used as a reference to compare the electrode performance. TEM images showed the 2–3-nm, well-dispered Pt particles on CBs.

The electrodes were prepared with the above HPt-CNT, KPt-CNT, and Pt-CB catalysts. The catalysts were dispersed in ethyl acetate followed by mixing with Nafion® 112 in ethyl acetate. The catalysts attached with Nafion® were cast, and two electrodes were formed. The two electrodes were separated by a Nafion® membrane.

I–V curves were measured with a circuit as shown in Fig. 1. The resistance can be changed and the current can be also checked with a propeller. Hydrogen and air were supplied to the anode and the cathode at 353 K, respectively, after bubbling in water at 353 K at atmospheric pressure. The hydrogen and oxygen was fed enough more than that providing maximum electromotive force.

IR spectra and transmission electron microscope (TEM) images were taken with FT/IR-600 (KBr beam splitter, JASCO) equipped with a reaction cell using ZnSe windows and JEM-2010F (JEOL), respectively. X-ray photoelectron (XP) spectra were acquired with Escalab 220i-XL (Vacuum Generator), and the Mg Kα line was used as the X-ray source. The elementary analysis data were acquired with Perkin-Elmer 2400 CHN Element Analyzer. Pt and metal catalyst for the CNT synthesis was measured as residue, and sulfur was absorbed by silver particles.

3. Results and discussion

Fig. 2 shows the *I–V* curves for the KPt-CNT, the HPt-CNT, and the Pt-CB electrodes. It was found that the Pt/CNT electrodes showed comparable performance as the Pt-CB electrodes in Fig. 2(a), where the KPt-CNT electrodes showed the highest voltages below 500 mA/cm^2 in Fig. 2(b). The power density as a function of the current density also showed the same tendency in Fig. 3. The higher voltages of the KPt-CNT suggest the formation of more effective triple-phase boundaries on the KPt-CNT electrodes than the other two electrodes, or the higher conductivity compared to the Pt/CB electrodes.

The CNTs used as electrodes were characterized by TEM as shown in Fig. 4. Fig. 4(a) revealed that the CNTs were the multi-walled carbon nanotubes (MWCNTs) with 20–50 nm diameters. Each layer of the CNT could be observed when TEM images were magnified as shown in Fig. 4(b). The graphene sheets are stacked parallel to the growth axis of carbon nanotubes, and their spacing was 0.34 nm as observed typically for MWCNTs [13].

The CNTs after Pt deposition were also observed by TEM. Fig. 5(a) shows the TEM image of the HPt-CNT. The small

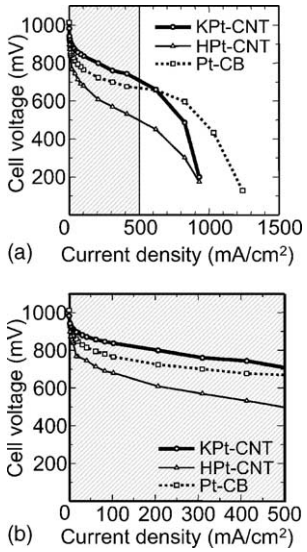

Fig. 2. *I–V* curves for the Pt-CB, the HPt-CNT, and the KPt-CNT electrodes. The *I–V* curves below 500 mA/cm^2 were enlarged in (b).

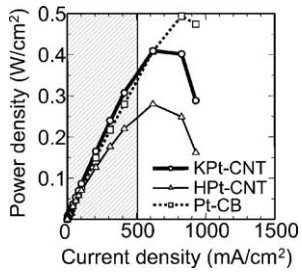

Fig. 3. Power current curves for the Pt-CB, the HPt-CNT, and the KPt-CNT electrodes.

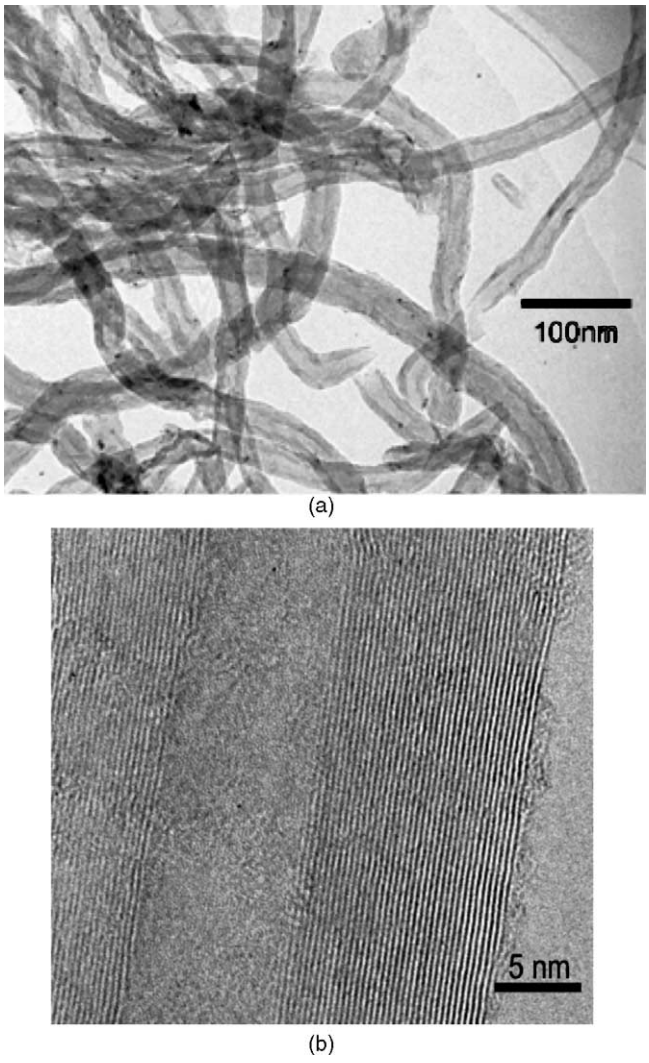

Fig. 4. TEM images of CNTs. (a) The shape of the CNTs. (b) The graphen layers of CNTs at different magnifications.

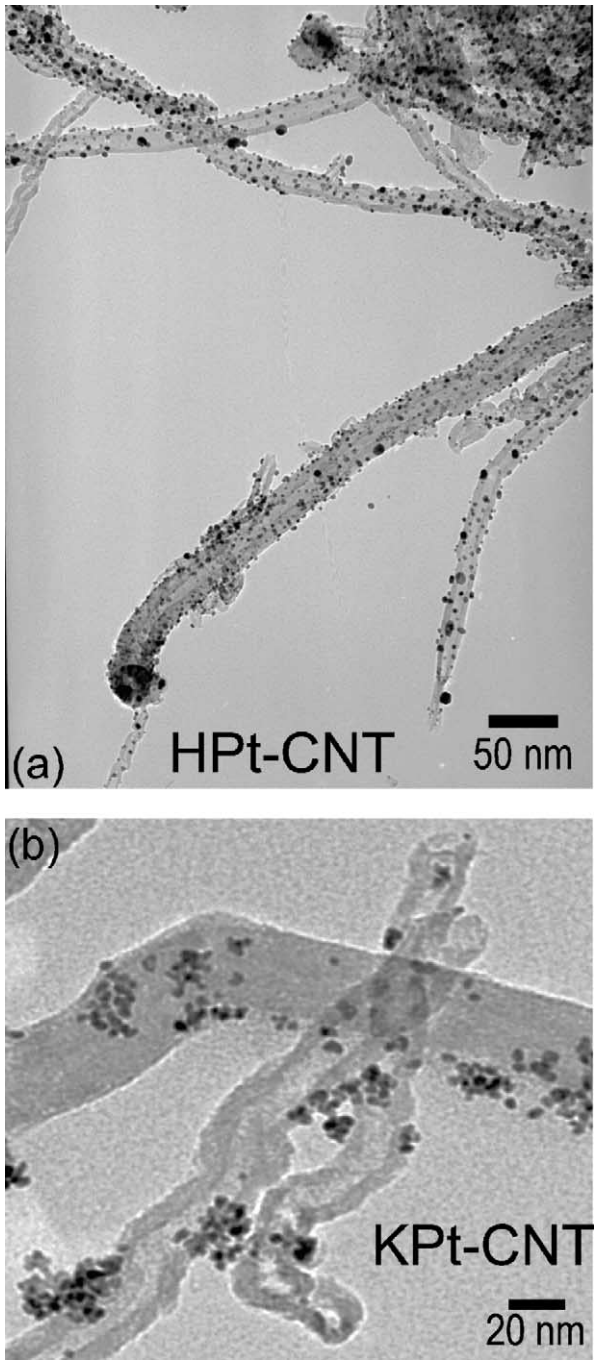

Fig. 5. TEM images Pt/CNT catalysts. (a) HPt-CNT. (b) KPt-CNT.

dark particles assigned to Pt particles were well dispersed on the CNT surfaces in the TEM image, while Pt particles were deposited locally and agglomerated each other on the KPt-CNT in Fig. 5(b). The diameters of the Pt particles range from 2 to 4 nm for both Pt/CNT catalysts. Pt ions can be reacted with the surface acid groups on the HPt-CNT surfaces [6]. The H_2PtCl_6 solution in ethylene glycol was yellow at 303–413 K, but became colorless at 473 K with producing Pt black. This indicates that the H_2PtCl_6 in ethylene glycol cannot be reduced to metallic Pt on the CNT surfaces at 413 K. That is why the Pt particles were directly attached and dispersed well on the CNT surfaces. On the other hand, the agglomeration of Pt particles shown in Fig. 5(b) may be ascribed to an autocatalytic decomposition of K_2PtCl_4 into metallic Pt particles. The initiators of the autocatalytic reaction can be the protons of the sulfate [14] or carboxyl groups [3,6], contaminations, defects or step edges on CNTs. The sulfate groups were observed by IR as discussed later. K_2PtCl_4 in the mixture of water and methanol was very unstable especially in light places and easily decomposed to produce Pt precipitations. The Pt particles thus catalyze the dissociation processes in the K_2PtCl_4 decomposition.

The functional groups on the KPt-CNT were investigated with IR to get information on the chemistry of the Pt deposition. The observed IR spectra are shown in Fig. 6. The Pt-CNT prepared using K_2PtCl_4 was heated at 373 and 623 K for 30 min in the FT-IR reaction cell with flowing He before observation. The background spectrum was obtained

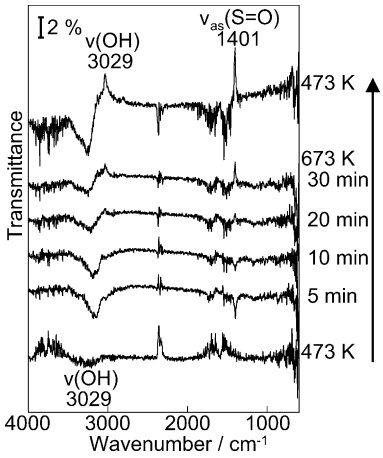

Fig. 6. IR spectra of the KPt-CNT in H_2. The background spectrum was obtained at 373 K after heating at 373 and 623 K for 30 min in He.

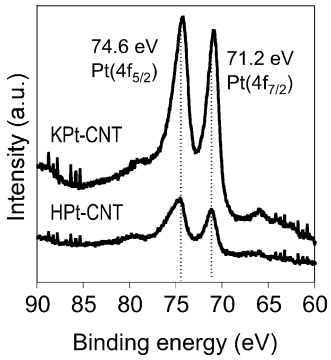

Fig. 7. XPS spectra of the HPt-CNT and the KPt-CNT catalysts.

at 373 K in He, and the sample spectra were observed at 473, 673, and 473 K again in H_2. The complicated features at 4000–3500, ~2400, and 1800–1500 cm^{-1} are due to the water vapor or CO_2 in the light path. Broad peaks appearing at 3400–3100 cm^{-1} are assigned to the O–H-stretching mode of the hydroxyl groups of alcohols and phenols [15–17]. When the KPt-CNT was heated at 673 K, the sharp peaks were observed at 3029 and 1401 cm^{-1} in 5 and 10 min, but the reverse peaks at the same frequencies grew in 20 and 30 min. These sharp peaks are assignable to the O–H and the asymmetric S=O-stretching modes of the OSO_3H groups as observed for aromatic sulfates [15–19]. The peaks became larger after cooling from 673 to 473 K due to the low sensitivity from the high background with the infrared irradiation at 673 K, and were unchanged during the observation at 473 K. It is thus clearly shown that the sulfate species is formed during the treatment of the CNTs with the mixed acid. The growth of the O–H-stretching mode of alcohols and phenols observed at 473 and 673 K is presumably due to the hydrogenation of carbonyl groups on the CNTs. The formation of the hydroxyl groups is not originated from the carboxyl groups, which are known to decompose at 373–673 K [20]. The peak broadness might be due to the various kinds of alcohol and phenol species because the frequency of the O–H-stretching mode shifts depending on the species to which the hydroxyl groups bond [15–17]. The increase of the sulfate peak intensity might be attributed to the conversion of the bidentate chelating sulfato compound to the monodentate sulfate with dehydration as observed on a sulfated ZrO_2 surface [19]. The reverse peaks at 3029 and 1401 cm^{-1} can be explained by the reduction of the sulfate groups with H spilled over from the metallic Pt particles as observed on the sulfated ZrO_2 surface at 673 K [21]. Here, we did not observe NO_2 groups expected with the nitration reaction [22].

The observation of the sulfate species by IR was consistent with the results of the elementary analysis showing 4.7, 0.2, and 14.0 wt.% for S, N, and metals, respectively. CNTs before Pt-deposition usually contain 1–2 wt.% metal catalysts to produce CNTs, and the Pt content is estimated to be 12–13 wt.%. This indicates that the sulfur compounds were formed more than the nitrogen compounds were on CNTs prepared with the mixed acids.

XPS spectra were measured to examine the state of Pt and the amount of Pt on the carbon supports. As shown in Fig. 7, Pt $4f_{5/2}$ and Pt $4f_{7/2}$ peaks appeared at 74.6 and 71.2 eV, respectively, indicating that the deposited Pt is metallic. The Pt content was estimated using XPS with taking the escape depth into account [23] as tabulated (Table 1). They were only 3.8 and 12 wt.% for the HPt-CNT and the KPt-CNT, respectively, while it was 29 wt.% for the Pt-CB. As for the KPt-CNT, the Pt content is consistent with the elementary analysis (12–13 wt.%). The Pt loads with the unit of mg/cm^2 and mg/W for the HPt-CNT, the KPt-CNT, and the Pt-CB were calculated with cast catalyst weight, electrode area, and Pt content. Table 1 includes the Pt loads of a current thin-Pt-film PEFC [1], the E-TEK commercial electrodes [24], and the Pt-deposited XC72R (CB) with using soluble electrolyte polymer Nafion® 117 [25]. It is shown that the KPt-CNT required the least Pt load to achieve the current PEFC performance below 500 mA/cm^2 and cut 60% Pt of the Pt-CB. On the other hand, the HPt-CNT electrode showed the best performance per Pt atom. It was indicated

Table 1
Pt content of electrode catalysts and Pt load of electrodes for PEFC.

	Pt content (wt.%)	Pt load (mg/cm^2)	Pt load (mg/W)	Reference
HPt-CNT	3.8	0.06	0.43	Present
KPt-CNT	12	0.2	1.0	Present
Pt-CB	29[a]	0.5	2.0	Present
Thin Pt film PEFC	–	0.6 (0.25[b])	1.5	[1]
E-TEK(CB)	20	0.4	1.5	[24]
XC72R (CB)	20	0.2 (0.25[c])	0.77	[25]
XC72R (CB)	20	0.11 (0.25[c])	0.70	[25]

[a] The Pt content of Pt-CB is announced by the distributor.
[b] 0.25 Pt mg/cm^2 to 0.12 Ru mg/cm^2 alloy is used for the anode.
[c] More Pt was used for the anode.

that MWCNTs are promising to reduce the Pt amount in the PEFC electrodes.

The voltages of the HPt-CNT were not high compared with the KPt-CNT, the Pt-CB or the current PEFCs, although small Pt particles are shown to be dispersed as shown in Fig. 5(a). The low voltages were due to the unsuccessful deposition procedure of Pt particles, which indicated that Pt-free CNTs were observed as many as the Pt-deposited CNTs. This might be due to the formation of CNT colloids after purification in HNO_3, and the Pt particles might be deposited only on the colloid surfaces. The mixed acid probably improves the Pt deposition uniformly on CNTs since Pt particles were attached to all the CNTs for the KPt-CNT. As for the KPt-CNT, the Pt load per power is worse than that of the HPt-CNT. This is presumably due to the agglomeration of Pt particles observed for the KPt-CNT. This seems to be unfavorable because the agglomeration is equivalent with formation of large particles with less triple-phase boundaries. The Pt-deposited XC72R gave the highest power at 1000 mA/cm^2, while the HPt-CNT and KPt-CNT gave at 600 mA/cm^2. The voltage drops of CNT electrodes from $\sim$600 mA/cm^2 might derive from the transportation limitation of oxygen, protons, or water [1]. This suggests that the improvement at higher current density is important for upgrading the present performance of these Pt/CNT catalysts.

In summary, the Pt/CNT electrodes gave two to four times higher performance per Pt atom than that of Pt/CB electrodes. The Pt/CNT electrodes prepared with K_2PtCl_4 gave the same voltages as a current PEFC at the least Pt load below 500 mA/cm^2. The Pt/CNT electrodes prepared with H_2PtCl_6 was found to have the potential to reduce Pt usage most because the Pt load per power overwhelmed the Pt/CNT electrodes prepared with K_2PtCl_4 or the other PEFC electrodes. These high performances of Pt/CNTs are considered to derive from the more efficient formation of triple-phase boundaries around dispersed Pt particles on the CNTs forming. The higher conductivity of CNTs is also considered to contribute to the high performance of the Pt/CNT electrodes. The Pt deposition is considered to accompany reactions with the function groups on CNTs or reduction on defective CNT surfaces. The CNT is a remarkable support for our Pt electrode catalysts below 500 mA/cm^2, and have the best potential to be used in commercial fuel cells with improvement at higher current density.

Acknowledgements

We acknowledge the discussion with Dr. Keishin Ohta at Microphase Co., Ltd, Japan and Dr. Lizhen Gao at Shenzhen University and contribution to the experiments of Mr. Keiji Kuroda at University of Tsukuba.

References

[1] EG&G Services, Parsons, Inc., Science Applications International Corporation, Fuel Cell Handbook, 5th ed., U.S. Department of Energy, Morgantown, 2002, pp. 3–6.
[2] W. Li, C. Liang, J. Qiu, W. Zhou, H. Han, Z. Wei, G. Sun, Carbon 40 (2002) 787.
[3] W. Li, C. Liang, W. Zhou, J. Qui, Z. Zhou, G. Sun, Q. Xin, J. Phys. Chem. B 107 (2003) 6292.
[4] M.C. Román-Martínes, D. Cazorla-Amorós, A. Linares-Solvano, C. Salinas-Martínez de Lecea, Carbon 33 (1995) 3.
[5] M.A. Fraga, E. Jordão, M.J. Medes, M.M. Freitas, J.L. Faria, J.L. Figueiredo, J. Catal. 209 (2002) 355.
[6] V. Lordi, N. Yao, J. Wei, Chem. Mater. 13 (2001) 733.
[7] S.D. Thompson, L.R. Jordan, M. Forsyth, Electrochemica Acta 46 (2001) 1657.
[8] T. Yoshitake, Y. Shimakawa, S. Kuroshima, H. Kimura, T. Ichihashi, Y. Kudo, D. Kasuya, K. Takahashi, F. Kokai, M. Yudasaka, S. Iijima, Physica B 323 (2002) 124.
[9] N. Choi, H. Kataura, S. Suzuki, Y. Achiba, Abstract of 23rd Fulleren-Nanotube Symposium, 2003, p. 134.
[10] J. Zhang, H. Zou, Q. Qing, Y. Yang, Q. Li, Z. Liu, X. Guo, Z. Du, J. Phys. Chem. B 107 (2003) 3712.
[11] T. Tada, M. Inoue, Yamamoto, 'Catalyst development for PEFC in Tanaka Kikinzoku Kogyo', Presented at 2001 International Seminar on Precious Metals, Hong Kong, March, 26–29.
[12] T. Tada, High dispersion catalysts including novel carbon supports, In: H. Gasteiger, A. Lamm (Eds.), Handbook of Fuel Cells, John Wiley & Sons, in press.
[13] P.M. Ajayan, In: H.S. Nalwa (Ed.), Nanostructured Materials and Nanotechnology, Concise edn., Academic Press, San Diego, 2002, Chapter 8, p. 332.
[14] X. Sun, R. Li, D. Villers, J.P. Dodelet, S. Désilets, Chem. Phys. Lett. 379 (2003) 99.
[15] K. Nakanishi, Infrared Absorption Spectroscopy, Holden-Day, Inc., San Francisco, 1962.
[16] K. Nakanishi, Infrared and Raman Spectra of Inorganic and Coordination Compounds, John Wiley & Sons, New York, 1986.
[17] C.J. Pouchert, The Aldrich Library of Infrared Spectra, Aldrich Chemical Company Inc., 1975.
[18] C. Morterra, G. Cerrato, F. Pinna, Spectrochim. Acta. A. 55 (1999) 95.
[19] F. Lange, K. Hadjiivanov, H. Schmelz, H. Knözinger, Catal. Lett. 16 (1992) 97.
[20] J.L. Figueiredo, M.F.R. Pereira, M.M.A. Freitas, J.J.M. Órfão, Carbon 37 (199) 1379, and reference therein.
[21] K. Ebitani, H. Konno, T. Tanaka, H. Hattori, J. Catal. 135 (1992) 60.
[22] J. Zawadzki, M. Wiśniewski, K. Skowrońska, Carbon 41 (2003) 235.
[23] T. Matsumoto, T. Komatsu, K. Arai, T. Yamazaki, M. Kijima, O. Shimizu, Y. Takasawa, J. Nakamura, Chem. Comm. (2004) 840.
[24] R.C. Urian, A.F. Gullá, S. Mukerjee, J. Electroanal. Chem. 554–555 (2003) 307.
[25] T.R. Ralph, G.A. Hards, J.E. Keoting, S.A. Campbell, D.P. Wilkinson, M. Davis, J. St-Pierre, M.C. Johnson, J. Electrochem. Soc. 144 (1997) 3845.